JOURNAL OF SOLID STATE CHEMISTRY 119, 80–89 (1995)

High-Temperature Transport and Defect Studies of Quadruple Perovskites: $La_2Ba_2Cu_2Sn_2O_{11}$, $Eu_2Ba_2Cu_2Ti_2O_{11}$, and $La_2Ba_2Cu_2Ti_2O_{11}$

P. A. Salvador, L. Shen, and T. O. Mason

Department of Materials Science and Engineering, Science and Technology Center for Superconductivity, Northwestern University, Evanston, Illinois 60208

and

K. B. Greenwood and K. R. Poeppelmeier

Department of Chemistry, Science and Technology Center for Superconductivity, Northwestern University, Evanston, Illinois 60208

Received September 15, 1994; in revised form March 27, 1995; accepted March 28, 1995

High temperature electrical conductivity and Seebeck coefficient measurements were performed on the quadruple perovskites $La_2Ba_2Cu_2Sn_2O_{11}$, $Eu_2Ba_2Cu_2Ti_2O_{11}$, and $La_2Ba_2Cu_2Ti_2O_{11}$. A transition from *n*- to *p*-type semiconductivity is observed for $La_2Ba_2Cu_2Sn_2O_{11}$ as a function of oxygen partial pressure. However, both electrons and holes contribute to the electrical properties over the entire range of experimental conditions. Both $Eu_2Ba_2Cu_2Ti_2O_{11}$ and $La_2Ba_2Cu_2Ti_2O_{11}$ display *p*-type extrinsic semiconductivity at high oxygen partial pressures and low temperatures. A transition to lightly doped *p*-type, intrinsic semiconductivity occurs at low oxygen partial pressures and high temperatures. Combined conductivity and thermopower (Jonker) analysis was employed to elucidate the defect structure and the conduction parameters in these compounds. The similarity of these materials to high-T_c cuprates is discussed. © 1995 Academic Press, Inc.

INTRODUCTION

It is widely recognized that high-T_c copper oxides consist of CuO_2 sheets interleaved between metal oxide layers which serve both as insulating separators and as charge reservoirs. However, several compounds containing copper–oxygen planes exist, including the quadruple perovskites (1–4), in which superconductivity has yet to be observed. This study was undertaken in an effort to establish whether a fundamental difference between the quadruple perovskites and other superconducting layered cuprates exists.

It is well established that defects, equilibrated at elevated temperatures, govern the electronic properties of layered cuprates. For instance, the carrier content on the CuO_2 planes is determined by oxygen defects and/or by aliovalent dopants. High temperature electrical measurements have been used to study both the defect structure and the normal state electrical properties of layered cuprates (5,6). Plots of the thermopower versus the logarithm of the conductivity, first developed by Jonker (7), have been used to analyze the conduction parameters in these materials (6). All of the high-T_c cuprates investigated displayed similar conduction parameters, and the superconducting compositions fell within a similar region on the Jonker curve (6). Figure 1 shows schematic Jonker curves representing $Bi_{2.1}Sr_{1.9}Ca_xY_{1-x}Cu_2O_8$ (Fig. 1A) $YBa_2Cu_3O_{7-\delta}$ (Fig. 1B), $La_{2-x}Ba_xCuO_4$ (Fig. 1C), and $Nd_{2-x}Ce_xCuO_4$ (Fig. 1D). Although portions of each curve are traced out as a function of doping, in each case, data for superconducting compositions lie near the high conductivity intercept (6, 8). Similar results have been obtained for other known superconductors such as $YBa_2Cu_4O_8$ (9) and $Y_{1-x}Ca_xSr_2Cu_2GaO_7$ (10), which suggests Jonker analysis is a powerful means for assessing the potential of other layered cuprates as superconducting materials.

The structure of the oxygen-deficient perovskite $La_2Ba_2Cu_2Sn_2O_{11}$ (1), illustrated in Figure 2, can be described by a tetragonal subcell of dimensions $1a_p \times 1a_p \times 4a_p$ (a_p, cubic perovskite cell dimension). Oxygen vacancy order results in a double copper–oxygen layer with square pyramidal coordination of the copper interleaved by a double tin–oxygen layer with octahedral coordination of the tin atoms. Although this material possesses the requisite CuO_2 layers, no evidence of superconductivity has been reported and attempts to dope this compound resulted in multiphase products (1). The lack of superconductivity in this material was attributed partly to the long in-plane copper–oxygen bond lengths, 2.00 Å, which are

0022-4596/95 $12.00

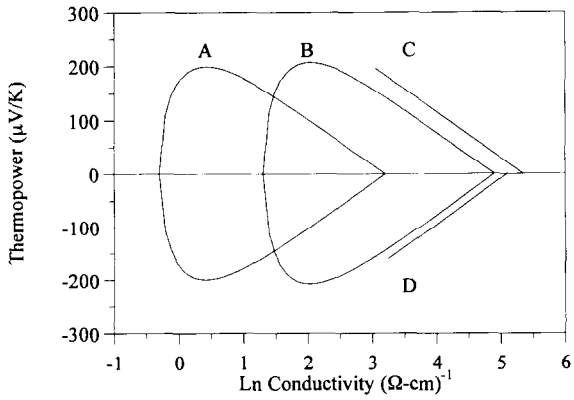

FIG. 1. Schematic representation of Jonker Data for $Bi_{2.1}Sr_{1.9}Ca_xY_{1-x}Cu_2O_8$ (A), $YBa_2Cu_3O_{7-x}$ (B), $La_{2-x}Ba_xCuO_4$ (C), and $Nd_{2-x}Ce_xCuO_4$ (D) from Refs. (5, 12).

~0.05 Å longer than those of high-T_c cuprates (1). Partial or complete replacement of tin by titanium can be achieved while maintaining the layered structure, if lanthanum is replaced by a smaller rare earth ion, i.e., $Ln_2Ba_2Cu_2Sn_{2-x}Ti_xO_{11}$ (2–4). Compounds adopting this structure include $Nd_2Ba_2Cu_2SnTiO_{11}$ (2), $Sm_2Ba_2Cu_2Sn_{0.5}Ti_{1.5}O_{11}$ (2), $Gd_2Ba_2Cu_2Ti_2O_{11}$ (3), and $Eu_2Ba_2Cu_2Ti_2O_{11}$ (4). The decrease in the size of the lanthanide and the replacement of tin by titanium results in a unit cell contraction, a reduction in the mismatch between the double Sn/Ti and Cu layers, and a decrease in the in-plane Cu–O bond length (2–4). The in-plane bond length of ~1.95 Å in $Gd_2Ba_2Cu_2Ti_2O_{11}$ (3) is similar to that of known superconductors, yet superconductivity has not been reported for the titanium-based quadruple perovskites. The stability of the layered structure in quadruple perovskites is reported to be extremely dependent on the size difference between the A and B cations (2–4). However, the structure of phases which do not meet the cationic size requirements for the layered structure have not been extensively reported. The instability of this structure may have important ramifications on the superconducting behavior of these compounds (i.e., the ability to introduce carriers by chemical doping).

This study focuses on the investigation of the conduction mechanisms and defect structures of quadruple perovskites. We report the structure of $La_2Ba_2Cu_2Ti_2O_{11}$, as determined by powder X-ray diffraction, a compound which is related to the layered quadruple perovskites by stoichiometry, but does not adopt an ordered layered structure. High-temperature electrical conductivity and thermopower measurements were conducted on $La_2Ba_2Cu_2Sn_2O_{11}$, $Eu_2Ba_2Cu_2Ti_2O_{11}$, and $La_2Ba_2Cu_2Ti_2O_{11}$. Jonker analysis was used to make comparisons between these materials and other layered cuprate systems. An understanding of these nominally undoped systems is essential if superconductivity is to be realized in the quadruple perovskites.

EXPERIMENTAL

Samples were prepared by the solid state reaction of stoichiometric amounts of barium carbonate (Aldrich, 99.999%), copper (II) oxide (Aldrich, 99.99+%), tin (IV) oxide (Aldrich, 99.995+%), titanium (IV) oxide (Aldrich, 99.99%), lanthanum oxide (Aldrich, 99.999%), and europium oxide (Aldrich, 99.99%). The reagents were ground and fired in high-density alumina boats at 950°C in air for 1 day. Each sample was air quenched, ground, and pressed into two pellets; one was less than 1 mm thick and the other was several millimeters thick. The pellets were then fired at 1010°C in air. The thin pellet was employed as a barrier to prevent diffusion of aluminum into the sample, while the large pellet was quenched, ground and fired several times during the course of a 7-day reaction period.

A Rigaku diffractometer with nickel filtered Cu$K\alpha$ radiation was employed to collect diffraction data on the quenched polycrystalline samples. Phase purity of the

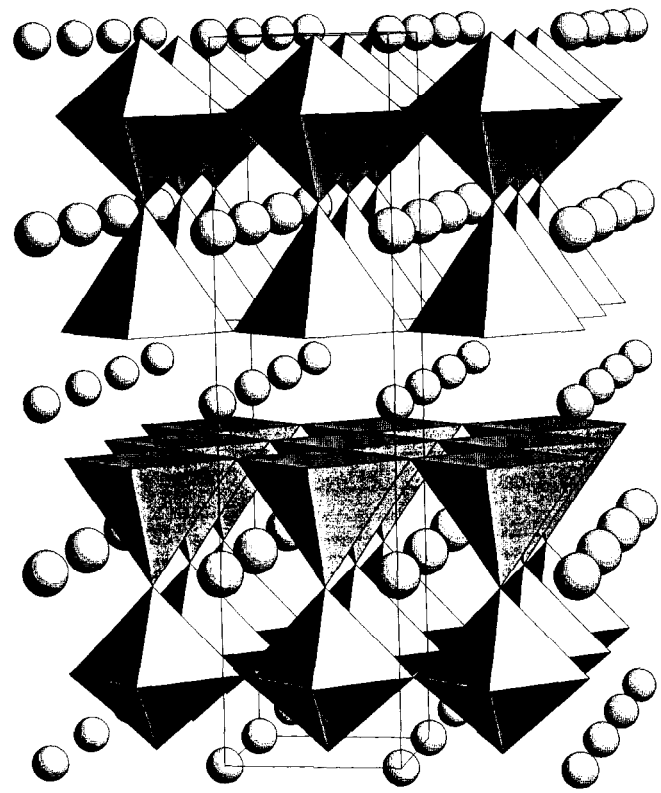

FIG. 2. Polyhedral representation of the idealized layered quadruple perovskite structure. The square pyramids are CuO_5, the octahedra are $(Sn/Ti)O_6$, the large spheres are barium sites, and the small spheres are the lanthanide sites.

samples was ensured by collecting data with a 2θ scan from 15° to 90° with a step of 0.02° and a collection time of 10 s at each step. Rietveld (11) analysis was used to determine the lattice parameters of the layered compounds and to refine the structure of $La_2Ba_2Cu_2Ti_2O_{11}$.

Hydrogen reduction thermogravimetry was performed using Dupont Instruments 951 and TA Instruments SDT 2960 thermogravimetric analyzers. $Eu_2Ba_2Cu_2Ti_2O_{11}$ and $La_2Ba_2Cu_2Ti_2O_{11}$ were heated to 900°C in an 8.5% H_2/91.5 % He atmosphere until an equilibrium weight was established, to reduce the compounds to known components which were identified by an X-ray diffraction trace.

Simultaneous four-point conductivity and thermoelectric coefficient measurements were made using the experimental apparatus described previously (12). The sintered pellets were sectioned into 2 × 2 × 8 mm conductivity bars and current contacts were established by pressing gold foil against the ends of the specimens. Voltage contacts consisted of gold wire looped around the bar and tied in place at notches along its length. One S-type thermocouple was in contact with each of the four leads, such that six thermocouple combinations could be used to register the steady state emfs and the corresponding temperature differences for thermoelectric coefficient measurements. A 15–30°C temperature gradient was maintained across the length of the specimen by placing it just off the hot zone in a controlled atmosphere furnace. A current reversal technique was employed to subtract out the thermal emf contributions. Flowing premixtures of oxygen and argon were used to vary the oxygen partial pressure above the sample, from 10^{-5} to 1 atm of oxygen, while the total pressure was maintained at 1 atm. Measurements were taken only after steady state had been achieved; typical equilibration times were 5–7 hr per datum.

TABLE 1
Powder X-Ray Diffraction Data of $Eu_2Ba_2Cu_2Ti_2O_{11}$ and $La_2Ba_2Cu_2Ti_2O_{11}$

$Eu_2Ba_2Cu_2Ti_2O_{11}$[a]						$La_2Ba_2Cu_2Ti_2O_{11}$[b]			
h	*k*	*l*	d_{obs}	d_{calc}	I_{obs}	*h* *k* *l*	d_{obs}	d_{calc}	I_{obs}
0	0	2	7.89	7.87	1				
0	0	3	5.25	5.25	<1				
0	0	4	3.935	3.936	8	1 0 0	3.943	3.940	15
1	0	0	3.891	3.890	17				
1	0	3	3.125	3.125	2				
1	0	4	2.767	2.767	100	1 1 0	2.786	2.786	100
1	1	0	2.751	2.751	46				
1	0	5	2.447	2.447	8				
1	1	3	2.437	2.436	1				
1	1	4	2.254	2.255	24	1 1 1	2.275	2.275	18
1	0	6	2.175	2.175	2				
0	0	8	1.968	1.968	10	2 0 0	1.969	1.970	29
2	0	0	1.945	1.945	32				
1	0	8	1.756	1.756	3	2 1 0	1.762	1.762	7
2	0	4	1.744	1.744	4				
2	1	0	1.741	1.740	4				
1	1	8	1.600	1.600	15	2 1 1	1.608	1.608	36
2	1	4	1.591	1.591	35				
2	1	5	1.523	1.523	3				
1	1	9	1.476	1.476	2				
2	0	7	1.472	1.471	2				
2	0	8	1.383	1.383	10	2 2 0	1.393	1.393	15
2	2	0	1.375	1.375	8				
1	0	11	1.343	1.343	3				
2	1	8	1.302	1.303	2	2 2 1	1.313	1.313	4
						3 0 0			
2	2	4	1.297	1.298	2				
1	0	12	1.243	1.243	3	3 1 0	1.246	1.246	14
1	2	9	1.234	1.234	1				
3	0	4	1.231	1.232	7				
3	1	0	1.229	1.230	7				
2	0	10	1.225	1.224	1				
3	0	5	1.199	1.199	1				

[a] $Eu_2Ba_2Cu_2Ti_2O_{11}$ was indexed on a $1a_p \times 1a_p \times 4a_p$ tetragonal cell with a = 3.8905 (3) Å and c = 15.744 (2) Å.

[b] $La_2Ba_2Cu_2Ti_2O_{11}$ was indexed on a $1a_p \times 1a_p \times 1a_p$ cubic cell with a = 3.9399 (3) Å (a_p is the lattice parameter for an ABO_3 perovskite).

RESULTS AND ANALYSIS

A. X-Ray Diffraction and Thermogravimetric Results.

Powder X-ray diffraction indicated that both $La_2Ba_2Cu_2Sn_2O_{11}$ and $Eu_2Ba_2Cu_2Ti_2O_{11}$ adopt the $1a_p \times 1a_p \times 4a_p$ layered quadruple perovskite structure, which is consistent with the literature (1, 4). However, $La_2Ba_2Cu_2Ti_2O_{11}$ did not adopt the layered quadruple perovskite structure. Table 1 compares the indexed powder diffraction pattern of $La_2Ba_2Cu_2Ti_2O_{11}$ with that of $Eu_2Ba_2Cu_2Ti_2O_{11}$. The diffraction data for $La_2Ba_2Cu_2Ti_2O_{11}$ can be indexed on a simple cubic perovskite cell, a = 3.9399(3) Å and was refined in space group $Pm\bar{3}m$. Lanthanum and barium were modeled as being distributed statistically over the *A*-site (site 1*b*) in the perovskite cell, while copper and titanium were distributed statistically over the *B*-site (site 1*a*). The oxygen content was fixed to the stoichiometric amount, as was confirmed by thermogravimetric results, and distributed statistically (site 3*d*) in the final refinement. Good agreement was reached between the observed and calculated intensities with this simple model (R_p = 5.68, R_{wp} = 7.54), despite the expectation of an ordered layered quadruple perovskite structure. As discussed by Gormezano and Weller (2), the cationic size differences in the lanthanum titanate are too large to stabilize a layered structure. Instead, the average structure can be described by a simple oxygen-deficient perovskite, where the different cations no longer adopt an ordered arrangement, but are distributed randomly (lanthanum and barium on the *A*-site, and copper and titanium on the *B*-site). The most significant feature of

this model is that the oxygen vacancies are distributed randomly throughout the oxygen sublattice, which forces both copper and titanium to adopt coordination numbers less than 6. However, the peaks for this compound are quite broad, which may indicate that the local structure is not described completely by the random perovskite model. Although this compound does not adopt a layered structure, we will refer to it as a random quadruple perovskite, with reference to the average structure and stoichiometry.

Thermogravimetric results indicate that the oxygen contents are stoichiometric, within experimental uncertainties, for all three compounds. The oxygen contents, as determined from an average of three reductions were 11.1 ± 0.1 and 11.0 ± 0.1 for $Eu_2Ba_2Cu_2Ti_2O_{11}$ and $La_2Ba_2Cu_2Ti_2O_{11}$, respectively. The reduction reaction for the thermogravimetric analysis of the titanates is

$$Ln_2Ba_2Cu_2Ti_2O_{11\pm\delta} + (2 \pm \delta)\, H_2 \rightarrow Ln_2O_3 + 2\, BaTiO_3 + 2\, Cu + (2 \pm \delta)\, H_2O, \quad [1]$$

where Ln = La or Eu. The reaction products were identified using powder XRD. The oxygen content of the layered stannate has been reported previously, along with the corresponding reduction reaction, and is 10.98 ± 0.05 (1). The statistical error in the measurements is too large to correlate with the electrical measurements, as discussed below, but confirms that structurally $\frac{1}{12}$ of the oxygen sites (of a normal perovskite) are vacant in all three compounds, including the random quadruple perovskite $La_2Ba_2Cu_2Ti_2O_{11}$.

B. Jonker Analysis and Conduction Mechanisms

Combined conductivity and thermopower analysis, first presented by Jonker (7), is briefly reviewed in order to analyze the electrical properties of the quadruple perovskites. Extensive mathematical treatment of Jonker plots is given elsewhere (6, 7), and only the salient features of the curves will be discussed below. In addition, the discussion will be limited to the symmetric case, i.e., conduction parameters (density of states, mobility, transport coefficient) for electrons and electron holes are identical. Jonker assumed a two-band, nondegenerate semiconductor model in order to derive a mathematical expression relating the thermopower to the natural logarithm of the conductivity. Three regions are apparent on the resulting curves, whose "pear" shapes have been demonstrated in Fig. 1. The first region corresponds to the intrinsic, undoped n to p transition and is associated with the region around the conductivity minimum, where the low conductivity intercept denotes the intrinsic conductivity. In this region, both electrons and holes contribute to the conductivity and thermopower. The other two regions correspond to extrinsic behavior, either n- or p-type, in which only a single carrier contributes to the conductivity and thermopower. These are denoted by linear regions on a Jonker pear with a slope of $-k/e$ for the acceptor-doped p-type "leg," and $+k/e$ for the donor-doped n-type "leg" (k is Boltzsman's constant and e is the unit of electronic charge).

The size and shape of the Jonker pear depends only on the intrinsic material parameters and can be expressed by the equation

$$\ln (2\sigma_{max}/\sigma_i) = (E_G/2kT + A) \quad [2]$$

where σ_i is the intrinsic conductivity, E_G is the band gap, k is Boltzman's constant, T is the temperature, and A is the transport coefficient (7). The transport coefficient can range from 0 to 4 depending on the primary scattering mechanism (13). Phonon scattering and small polaron conduction have been theorized to play important roles in layered cuprates at elevated temperatures (8–10, 14), where the values of A are 0 and 2, respectively. The usefulness of Jonker's approach is that data spanning only a portion of the pear is often sufficient to determine the transport parameters of a material (7).

The high conductivity intercept, σ_{max}, can be related to the transport parameters as follows:

$$\sigma_{max} = N\mu e e^A. \quad [3]$$

The temperature dependence of this value can provide additional information about the mobility of the carriers. For a two-band conductor, the temperature dependence of the density of states, N, and mobility, μ, are such that they approximately cancel in the term on the right-hand side of Eq. [3]. This results in a temperature-independent high conductivity intercept (7). Because of their activated mobility, small polarons exhibit a temperature-dependent high conductivity intercept (7) unless the hopping energy is on the order of kT (9), in which case a temperature-independent intercept results. Thus, small polaron conduction can be distinguished only if the high conductivity intercept is temperature dependent.

Jonker plots for $La_2Ba_2Cu_2Sn_2O_{11}$, $Eu_2Ba_2Cu_2Ti_2O_{11}$, and $La_2Ba_2Cu_2Ti_2O_{11}$ are shown in Figs. 3–5, respectively. $La_2Ba_2Cu_2Sn_2O_{11}$ exhibits n-type behavior, i.e., negative thermopower values, at low oxygen partial pressures and transitions to p-type behavior as the oxygen partial pressure is increased. The value of the oxygen partial pressure at the point of zero thermopower increases from log $pO_2 \approx -2.5$ at 650°C, to log $pO_2 \approx -1.5$ at 800°C. Intrinsic behavior is observed over the entire range of experimental conditions, indicating that both electrons and electron holes are contributing to the thermopower and conductivity in $La_2Ba_2Cu_2Sn_2O_{11}$. Figures 4 and 5 prove that this

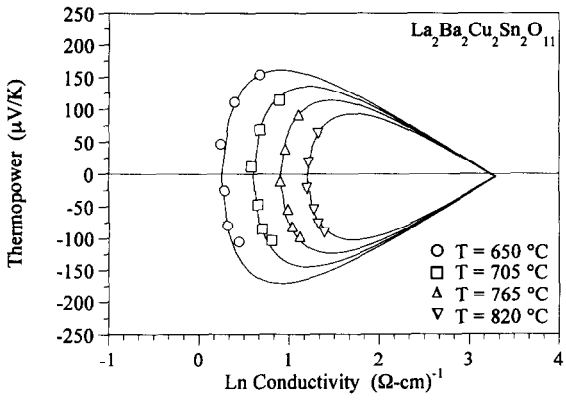

FIG. 3. Jonker analysis of thermopower and conductivity data for $La_2Ba_2Cu_2Sn_2O_{11}$ at four temperatures. Data at each temperature correspond to oxygen partial pressures of 10^{-5}, 10^{-4}, 10^{-3}, 10^{-2}, 10^{-1}, and 10^{0} atm, in a counterclockwise fashion.

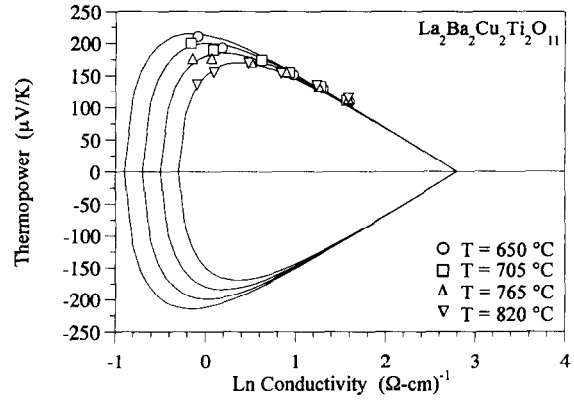

FIG. 5. Jonker analysis of thermopower and conductivity data for $La_2Ba_2Cu_2Ti_2O_{11}$ at four temperatures. Data at each temperature correspond to oxygen partial pressures of 10^{-5}, 10^{-4}, 10^{-3}, 10^{-2}, 10^{-1}, and 10^{0} atm, in a counterclockwise fashion.

is not the case for $Eu_2Ba_2Cu_2Ti_2O_{11}$ and $La_2Ba_2Cu_2Ti_2O_{11}$. At high oxygen partial pressures, the titanate systems exhibit extrinsic, *p*-type conductivity. As the oxygen partial pressure is lowered, the data moves up the *p*-type extrinsic leg of the pear. At high temperatures and low oxygen partial pressures, both systems transition from extrinsic behavior to lightly doped *p*-type behavior. $La_2Ba_2Cu_2Ti_2O_{11}$ exhibits extrinsic behavior over a larger range of oxygen partial pressures, however, and displays only a slight deviation from extrinsic behavior at the lowest oxygen partial pressures.

Each set of data in Figs. 3–5 was fitted with a calculated Jonker curve. Both the intrinsic conductivity, σ_i, and the maximum conductivity, σ_{max}, were obtained from the fitted Jonker curves. The gap energy can be calculated using Eq. [2] and the values found from the fitted Jonker curves if we assume a value for the transport constant, *A*. Table 2 lists the values of E_G, for the phonon scattering (A = 0) and small polaron (A = 2) cases, as well as ln σ_i and ln σ_{max}. The gap energies for the tin system, ranging from 0.15 to 0.28 for band conduction and 0.53 to 0.60 for small polaron conduction, are similar to those values reported for $La_3Ba_3Cu_6O_{12.5+y}$ (LBC-336) (6). The gap energies in the titanates are larger than those for $La_2Ba_2Cu_2Sn_2O_{11}$ and LBC-336, but slightly smaller than have been reported for $YBa_2Cu_3O_{6+y}$ (YBC-123) (6). The similarities among LBC-336, YBC-123, and the quadruple perovskites are striking and will be discussed in more detail below.

The values in Table 2 demonstrate that ln σ_{max} is temperature independent for all three materials, indicating itinerant carriers or small polarons with activation energies on

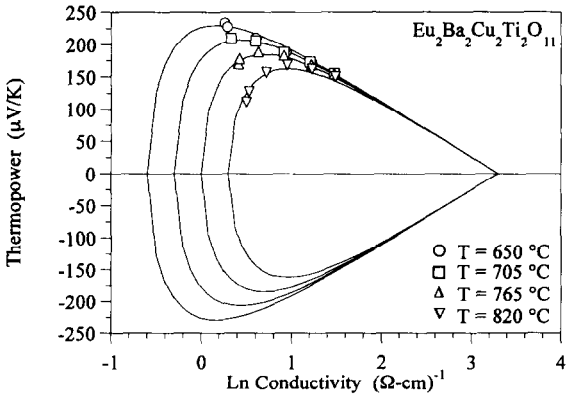

FIG. 4. Jonker analysis of thermopower and conductivity data for $Eu_2Ba_2Cu_2Ti_2O_{11}$ at four temperatures. Data at each temperature correspond to oxygen partial pressures of 10^{-5}, 10^{-4}, 10^{-3}, 10^{-2}, 10^{-1}, and 10^{0} atm, in a counterclockwise fashion.

TABLE 2
Fit Parameters and Intrinsic Gap Energies from Jonker Analysis

			E_g (eV)	
T (K)	ln σ_i	ln σ_{max}	Band	Small polaron
		$La_2Ba_2Cu_2Sn_2O_{11}$		
923	0.25	3.3	0.28	0.60
978	0.60	3.3	0.23	0.57
1038	0.90	3.3	0.20	0.55
1093	1.20	3.3	0.15	0.53
		$Eu_2Ba_2Cu_2Sn_2O_{11}$		
923	−0.60	3.3	0.41	0.73
973	−0.30	3.3	0.38	0.72
1023	0.00	3.3	0.35	0.70
1073	0.30	3.3	0.31	0.68
		$La_2Ba_2Cu_2Ti_2O_{11}$		
923	−0.90	2.8	0.38	0.70
973	−0.70	2.8	0.37	0.70
1023	−0.50	2.8	0.35	0.70
1073	−0.30	2.8	0.33	0.70

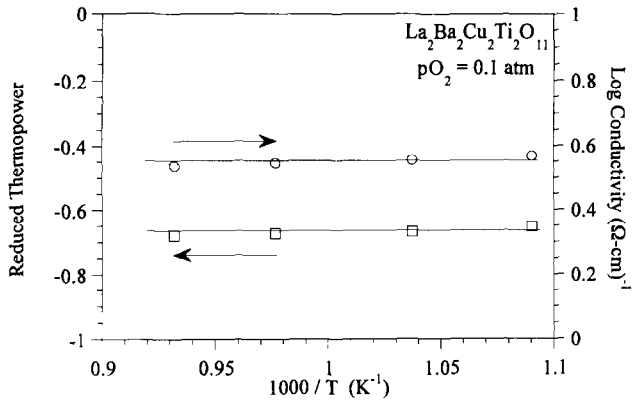

FIG. 6. Reduced thermopower and conductivity versus inverse temperature for $La_2Ba_2Cu_2Ti_2O_{11}$ at an oxygen partial pressure of 10^{-1} atm.

the order of kT or less. Additional evidence of a temperature-independent mobility in these materials is given in Fig. 6, which is a plot of reduced thermopower and the logarithm of conductivity versus inverse temperature for $La_2Ba_2Cu_2Ti_2O_{11}$ at an oxygen pressure of 0.1 atm. The reduced thermopower, Q_r, and the logarithm of the conductivity, σ, for an extrinsic p-type semiconductor are given by

$$Q_r = -eQ/2.303k = \log p - \log N + A/2.303 \quad [4]$$

and

$$\log \sigma = \log p + \log e\mu \quad [5]$$

respectively, where p is the hole concentration. The slope of the reduced thermopower is nearly zero as a function of inverse temperature, indicating that the concentration of holes is nearly constant over this temperature range. The observation that the logarithm of conductivity is also temperature independent indicates that the mobility is nonactivated over the same temperature range. Similar behavior is observed for $Eu_2Ba_2Cu_2Ti_2O_{11}$ in the extrinsic p-type regime. This behavior is illustrated in Figs. 4 and 5, at high oxygen partial pressures, where the data for all four temperatures become coincidental. This analysis does not preclude the existence of small polarons, but sets an upper limit for the activation energy, $E_h \approx kT$, as was concluded in $La_{2-x}Ba_xCuO_4$ (8) and $YBa_2Cu_3O_{6+y}$ (8, 14).

C. Defect Structure Analysis

The following discussion assumes that the stoichiometric composition is the reference composition, i.e., the intrinsic composition, for all three compounds. Plots of the logarithm of conductivity versus the logarithm of oxygen partial pressure are shown in Figs. 7a and 7b for the titanate systems at 650 and 800°C, respectively. A line of slope $+\frac{1}{6}$ fits the data for both systems at 650°C, indicative of a p-type material. A slight deviation from the $+\frac{1}{6}$ slope occurs for $Eu_2Ba_2Cu_2Ti_2O_{11}$ at the lowest oxygen partial pressure, to a region of lower slope. This deviation is more pronounced in the data collected at 800°C and can be understood as a transition from an extrinsic semiconductor to a lightly doped intrinsic semiconductor, as was seen in Fig. 4. The data for $La_2Ba_2Cu_2Ti_2O_{11}$ exhibits a $+\frac{1}{6}$ slope over the entire range of experimental conditions, which is consistent with extrinsic behavior being predominant for this material, as was seen in Fig. 5.

The extrinsic behavior of these materials is similar to that reported for $La_2CuO_{4+\delta}$ (5, 15). In this related cuprate, electrical properties which are proportional to the $+\frac{1}{6}$ power of the oxygen partial pressure have been attributed to the presence of oxygen interstitials according to

$$\tfrac{1}{2}\,O_2(g) \leftrightarrow O_i'' + 2h^{\cdot}, \; K_{ox}pO_2^{1/2} = [O_i'']p^2. \quad [6]$$

The electroneutrality condition in this regime is given by

$$p = 2[O_i''], \quad [7]$$

which, when Eqs. [6] and [7] are solved simultaneously for the hole concentration, results in the observed $+\frac{1}{6}$ slope dependence. This indicates that both $La_2Ba_2Cu_2Ti_2O_{11}$ and $Eu_2Ba_2Cu_2Ti_2O_{11}$ are oxygen excess materials at low temperatures and high oxygen partial pressures. In addition, the temperature-independent behavior of the thermopower in the extrinsic region, seen in Fig. 6, argues that the oxygen interstitial population is not a strong function of temperature, but is fixed by the oxygen partial pressure, as in $La_2CuO_{4+\delta}$ (15). The main difference between the titanates and $La_2CuO_{4+\delta}$ is that the copper titanates exhibit a transition into an intrinsic region not seen in $La_2CuO_{4+\delta}$. The plateau observed in the conductivity at low oxygen partial pressures for $Eu_2Ba_2Cu_2Ti_2O_{11}$ indicates that interstitial oxygen ions are no longer a majority species. The defect structure in this regime can be modeled with an intrinsic electronic defect mechanism,

$$\text{null} \leftrightarrow e' + h^{\cdot}, \quad K_i = np, \quad [8]$$

and an anionic Frenkel pair reaction,

$$O_O^x \leftrightarrow V_O^{\cdot\cdot} + O_i'', \quad K_f = [V_O^{\cdot\cdot}][O_i''], \quad [9]$$

where K_i and K_f are the equilibrium constants for the intrinsic reaction and the Frenkel reaction, respectively. If $K_i \gg K_f$, then the electroneutrality condition will be given by,

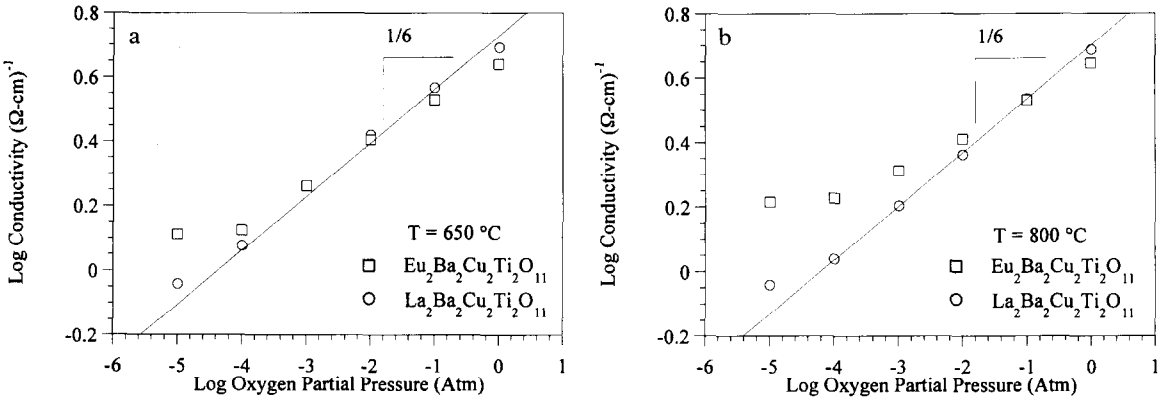

FIG. 7. Logarithm of conductivity versus the logarithm of oxygen partial pressure for $Eu_2Ba_2Cu_2Ti_2O_{11}$ and $La_2Ba_2Cu_2Ti_2O_{11}$ at (a) 650°C and (b) 800°C.

$$n = p, \qquad [10]$$

and the conductivity will be independent of the oxygen partial pressure. However, if $K_i \ll K_f$, then the electroneutrality condition will be given by

$$[O_i''] = [V_O^{\cdot\cdot}], \qquad [11]$$

and, when substituted into Eq. [6], the hole concentration is found to have a $+\frac{1}{4}$ power dependence on oxygen partial pressure. The prior case, $K_i \gg K_f$, is supported by the data shown in Fig. 7b, where a region of near zero slope transitions directly into a region of $+\frac{1}{6}$ slope as oxygen partial pressure is increased. This corresponds to the transition from a region where the electroneutrality is given by Eq. [10] to a region where it is given by Eq. [7]. In addition, K_i is temperature dependent (see gap energies in Table 2) but K_{ox} has been determined to be temperature independent, thus causing flattening of the conductivity to occur at higher oxygen partial pressures as temperature is increased. This model is in excellent agreement with the experimental data for both layered titanates. $La_2Ba_2Cu_2Ti_2O_{11}$ exhibits only a small deviation, owing to the persistence of extrinsic behavior in this material. This indicates that either K_i is smaller or K_{ox} is greater in the random system as compared with the layered system. The gap energies, see Table 2, are quite similar between the two systems and therefore the density of states would have to be smaller in the random titanate to explain the observed behavior. Alternatively, the random arrangement of oxygen vacancies in the structure of $La_2Ba_2Cu_2Ti_2O_{11}$ may facilitate the incorporation of excess oxygen, thus increasing K_{ox} relative to $Eu_2Ba_2Cu_2Ti_2O_{11}$, where the smaller europium ion occupies the cationic site in the plane of the ordered oxygen vacancies.

A defect model for the layered copper stannate cannot be as clearly ascertained from the available electrical data. The Jonker behavior of this compound has shown that electrons and holes are contributing to the thermopower and conductivity over the entire range of oxygen partial pressures investigated. However, nearly the entire intrinsic regime is traversed in six orders of magnitude of oxygen partial pressure. The logarithm of conductivity for $La_2Ba_2Cu_2Sn_2O_{11}$ is plotted as a function of the logarithm of oxygen partial pressure in Fig. 8. The figure demonstrates that there is a slight dependence of the conductivity on oxygen partial pressure. If the same model is used for the intrinsic regime as for the layered titanate, Eqs. [8] and [9], the observed behavior is best described if K_i is slightly larger than K_f. The region of zero slope, corresponding to the neutrality condition in Eq. [10], exists only over a narrow region of oxygen partial pressure, and transitional slopes are observed as the material moves into the extrinsic regimes. Although the electrical data qualitatively fits the defect model presented, precise oxygen content determination as a function of the oxygen

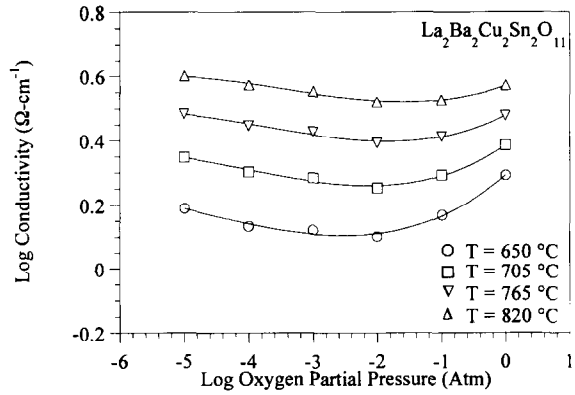

FIG. 8. Logarithm of conductivity versus the logarithm of oxygen partial pressure for $La_2Ba_2Cu_2Sn_2O_{11}$ at four temperatures.

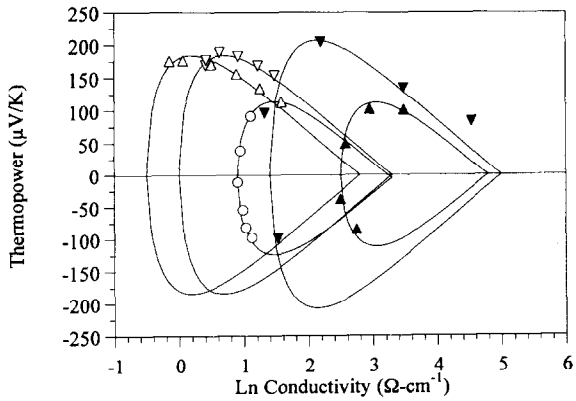

FIG. 9. Jonker plots for $La_2Ba_2Cu_2Sn_2O_{11}$ (○), $Eu_2Ba_2Cu_2Ti_2O_{11}$ (▽), $La_2Ba_2Cu_2Ti_2O_{11}$ (△), $La_3Ba_3Cu_6O_{14\pm\delta}$ (▲) (Ref. 6), and $YBa_2Cu_3O_{6+x}$ (▼) (Ref. 6) at a temperature of ~760°C.

partial pressure must be undertaken to verify this model. This work is currently underway.

DISCUSSION

The high-temperature electrical properties of the quadruple perovskites are not significantly different from other layered cuprates. As mentioned previously, the Jonker behavior of these "undoped" systems is remarkably similar to the behavior of LBC-336 and YBC-123. Figure 9 is a Jonker plot of the data collected in the present investigation along with data from the 123-type compounds. It is clear from the figure that $La_2Ba_2Cu_2Sn_2O_{11}$ and LBC-336 are remarkably similar, except that the density of states-mobility product is slightly smaller in the quadruple perovskite. Both display an amphoteric nature which is dependent on the oxygen partial pressure. However, LBC-336 traces a larger portion of the pear, and transitions to an extrinsic *p*-type semiconductor at high oxygen partial pressure. $LaBa_2Cu_3O_{6+y}$ (LBC-123), which can be derived stoichiometrically from LBC-336 by replacing 25% of the lanthanum with barium, also exhibits similar behavior (17) but extends further down the *p*-type extrinsic leg. The titanate systems exhibit behavior intermediate between LBC-336 and YBC-123. Despite displaying both lightly doped intrinsic and extrinsic *p*-type conductivity, as do LBC-336 and YBC-123, the titanates are confined to a much smaller region of the pear. Both LBC-123 and YBC-123 can be made to superconduct by oxygen annealing, while LBC-336 is nonsuperconducting. The two superconducting systems display extensive *p*-type extrinsic behavior, whereas LBC-336 and the quadruple perovskites are confined to the regions near the base of the pear. This indicates that the number of charge carriers in the nonsuperconducting compounds is much lower than that in the superconducting compositions. Efforts to increase the number of charge carriers in the layered quadruple perovskites have not yielded single-phase materials (1). Aliovalent substitution of lanthanum with barium in LBC-336 results in LBC-123, as mentioned above, yet despite the drastic change in cationic composition oxygen treatment is still required to optimize superconductivity. The similarity of the high-temperature electrical properties of the quadruple perovskites to these systems indicates that strict control of both anionic and cationic compositions will be required to realize superconductivity in these materials.

There are several structural differences between the quadruple perovskites and the 123 systems. Most importantly, the inorganic spacer layer in the 123-type systems contains a copper ion, capable of both variable valence states and oxygen coordination.The inorganic spacer layers in the present materials contain either titanium or tin, both of which prefer a valence state of +4 and octahedral coordination by oxygen. These preferences have been attributed to the stability of the layered quadruple perovskite structure (1–4). The oxygen nonstoichiometry in these materials is therefore expected to be confined to a narrower range than that seen in the 123-type systems, which is consistent with the Jonker behavior and previous thermogravimetric studies (1–4), indicating essentially stoichiometric oxygen contents. However, oxygen intercalation between double copper–oxygen sheets, similar to those in the quadruple perovskites, has been observed in $La_{2-x}Sr_{1+x}Cu_2O_{6+\delta}$ (18, 19) and $La_{2-x}Sr_xCaCu_2O_{6+\delta}$ (20, 21). In addition, oxygen vacancies in the CuO_2 plane along with oxygen intercalation between these planes has been observed in $Eu_{1.3}Sr_{1.7}Cu_2O_{6-\delta}$ (22) and $Nd_{2-x}Sr_{1+x}Cu_2O_{6-\delta}$ (23, 24). Therefore, oxygen excess or disorder on the oxygen sublattice, as proposed in the above defect model, is not unexpected in quadruple perovskites. The ionic defects are too small in number to increase the carrier content to appropriate levels for superconductivity, but must be considered as effective compensation mechanisms to electronic defects. Further investigation of the oxygen stoichiometry as a function of oxygen partial pressure is underway.

The question of disorder on the oxygen sublattice is most pertinent to $La_2Ba_2Cu_2Ti_2O_{11}$. Powder X-ray diffraction indicates that copper and titanium are randomly distributed on the *B*-site of this cubic perovskite. In addition, oxygen vacancies are randomly distributed on the oxygen sublattice, requiring a large number of titanium ions to be coordinated by less than six oxygens. An excessive number of vacancies around titanium ions would seem energetically unfavorable for this compound. Peak broadening in the diffraction data could be an indication of an ordered local structure undetectable by powder X-ray diffraction. The similarity in the high-temperature electrical properties of the layered copper titanate and the ran-

dom copper titanate is remarkable. The persistence of an interstitial oxygen defect mechanism at the boundary of the intrinsic electronic regime argues that the electronic disorder is greater than the ionic disorder in the intrinsic regime, as seen in the layered titanate. However, this compound is a highly oxygen-deficient perovskite, containing 8.33% oxygen vacancies with respect to the ideal perovskite stoichiometry. Therefore, the large number of oxygen vacancies in this material must be considered a structural feature, and the electronic behavior is determined from the reference state with an oxygen stoichiometry of 11, as mentioned above. The similarity of the two titanate systems indicates either that the high-temperature electronic behavior of these polycrystalline cuprates is not strongly correlated to their layered structure or that the local structure of the two compounds is more closely related than powder XRD indicates. Electron microscopy is underway to investigate the latter.

The *n*-type behavior of $La_2Ba_2Cu_2Sn_2O_{11}$ is not suprising when considering the long in-plane copper–oxygen bond length. Similar behavior in the 123-systems is difficult to correlate with the in-plane bond lengths because of the multiple copper sites available. The decrease in this bond length for the layered titanate seems to stabilize *p*-type behavior. However, the intrinsic behavior indicates that holes and electrons are present in both systems. Stabilizing doped samples has been unsuccessful to date, which can be attributed to several features of these materials. A delicate balance exists between the cationic sizes and the stabilization of the layered structure (1–4), and the introduction of charged species serves to further complicate this balance. In addition, ionic defects are an important feature of these compounds, as seen with the electrical properties, which compete with electronic compensation mechanisms when aliovalent impurities are introduced. Careful consideration must be given to the preferences in coordination and valence, as well as the size, of potential dopant ions such that the layered structure can be maintained and the generation of electronic carriers is the predominant compensation mechanism. High-temperature electrical investigations of doped samples are currently being pursued.

CONCLUSIONS

High-temperature electrical characterization of quadruple perovskites has demonstrated that both electronic and ionic defects play an important role in these compounds. $La_2Ba_2Cu_2Sn_2O_{11}$ displays an *n* to *p* transition as a function of oxygen partial pressure, but the intrinsic generation of electron–hole pairs dominates the conductivity of this semiconductor. $Eu_2Ba_2Cu_2Ti_2O_{11}$ and $La_2Ba_2Cu_2Ti_2O_{11}$ both are *p*-type extrinsic semiconductors at high oxygen partial pressures and low temperatures. The defect structure in this regime is dominated by interstitial oxygen defects, i.e., $p = 2[O_i'']$. At low oxygen partial pressures and high temperatures a transition occurs to lightly doped *p*-type semiconductivity, where both electrons and holes contribute to the electrical properties. In this region, the electroneutrality condition becomes that of an intrinsic semiconductor, $n = p$. The complete substitution of europium by lanthanum in $Eu_2Ba_2Cu_2Ti_2O_{11}$ destabilizes the layered quadruple perovskite structure. The average structure of $La_2Ba_2Cu_2Ti_2O_{11}$ is that of a simple, oxygen-deficient, cubic perovskite which does not contain a CuO_2 layer. Jonker analysis indicates that the layered quadruple perovskites are similar to superconducting layered cuprates in their high-temperature electrical behavior, yet the total carrier content is well below that of known superconductors. If doping mechanisms which increase the number of carriers, while maintaining the layered structure, can be realized, superconductivity may be attainable in this class of compounds.

Note added in support. Since the submission of this manuscript, a structural investigation of $La_2Ba_2Cu_2Ti_2O_{11}$, using powder X-ray and neutron diffraction, has been reported (25). Whereas X-ray diffraction indicates no long-range order, and the data are sufficiently described by the cubic perovskite structure, neutron diffraction confirms the existence of partial order in this compound (25). The neutron results were successfully modeled using two ordered microdomains with the same crystal structure but displaced origins (25). Although the order does not extend to long range, it does preserve the local environment of the copper and titanium cations, in two microdomains distributed throughout the bulk. These results agree well with our observations and conclusions: the broad cubic perovskite peaks from X-ray diffraction and similar high-temperature electrical properties to the layered quadruple perovskite, $Eu_2Ba_2Cu_2Ti_2O_{11}$, imply local order in $La_2Ba_2Cu_2Ti_2O_{11}$. The similarity of the defect chemistry in the two titanate systems can therefore be attributed to the similarity of the local structure in these layered quaternary perovskites.

ACKNOWLEDGMENTS

This work was supported by the Science and Technology Center for Superconductivity under NSF Grant DMR-91-20000 (P.A.S., K.B.G., T.O.M., K.R.P.). The authors also acknowledge the support of the U.S. Department of Energy under Grant FG02-84ER45097 (L.S., T.O.M.). This work made use of MRC central facilities supported by the National Science Foundation, at the Materials Research Center of Northwestern University, under Award DMR-9120521. The authors also thank Bruce J. Hinds and Tobin J. Marks for their assistance with the thermogravimetric studies.

REFERENCES

1. M. T. Anderson, K. R. Poeppelmeier, J.-P. Zhang, H.-J. Fan, and L. D. Marks, *Chem. Mater.* **4**, 1305 (1992).

2. A. Gormezano and M. T. Weller, *J. Mater. Chem.* **3**(9), 979 (1993).
3. A. Gormezano and M. T. Weller, *J. Mater. Chem.* **3**(7), 771 (1993).
4. K. B. Greenwood, M. T. Anderson, K. R. Poeppelmeier, D. L. Novikov, A. J. Freeman, B. Dabrowski, S. A. Gramsch, and J. K. Burdett, *Physica C,* in press.
5. T. O. Mason, *in* "Electronic Ceramic Materials" (J. Nowotny, Ed.), p. 502. Trans Tech Publications, Zurich, 1992.
6. M.-Y. Su, C. E. Elsbernd, and T. O. Mason, *J. Am. Ceram. Soc.* **73**(2), 415 (1990).
7. G. H. Jonker, *Philips Res. Rep.* **23,** 131 (1968).
8. M.-Y. Su, C. E. Elsbernd, and T. O. Mason, *Physica C* **160,** 114 (1989).
9. B.-S. Hong and T. O. Mason, *Solid State Ionics* **49,** 3 (1991).
10. G. W. Tomlins, N.-L. Jeon, T. O. Mason, D. A. Groenke, J. T. Vaughey, and K. R. Poeppelmeier, *J. Solid State Chem.* **109,** 338 (1994).
11. D. B. Wiles, A. Sakthivel, and R. A. Young, "Rietveld Analysis Program DBWS-9006PC." School of Physics, Georgia Institute of Technology, 1990.
12. A. Trestman-Matts, S. E. Dorris, and T. O. Mason, *J. Am. Ceram. Soc.* **66**(8), 589 (1983).
13. A. F. Joffe, "Physics of Semiconductors." Infosearch, Ltd., London, UK, 1960.
14. M.-Y. Su, K. Sujata, and T. O. Mason, *in* "Ceramic Superconductors II" (M. F. Yan, Ed.), p. 99, American Ceramic Society, Westerville, Ohio, 1988.
15. M.-Y. Su, E. A. Cooper, C. E. Elsbernd, and T. O. Mason, *J. Am. Ceram. Soc.* **73**(11), 3453 (1990).
16. M. Y. Su, S. E. Dorris, and T. O. Mason, *J. Solid State Chem.* **75,** 381 (1988).
17. B.-S. Hong and T. O. Mason, *in* "Ceramic Transactions, Volume 18, Superconductivity and Ceramic Superconductors II" (K. M. Nair, U. Balachandran, Y.-M. Chiang, and A. S. Bhalla, Eds.), p. 95, American Ceramic Society, Westerville, OH, 1991.
18. P. Lightfoot, S. Pei, J. D. Jorgenson, X.-X. Tang, A. Manthiram, and J. B. Goodenough, *Physica C* **169,** 464 (1990).
19. V. Caignaert, N. Nguyen, and B. Raveau, *Mater. Res. Bull.* **25,** 199 (1990).
20. A. Fuertes, X. Obradors, J. M. Navarro, P. Gómez-Romero, N. Casañ-Pastor, F. Pérez, J. Fontcuberta, C. Miravitlles, J. Rodríguez-Carvajal, and B. Martínez, *Physica C* **170,** 153 (1990).
21. T. Sakurai, T. Yamashita, J. O. Willis, H. Yamauchi, and S. Tanaka, *Physica C* **174,** 187 (1991).
22. N. Nguyen, J. Choisnet, and B. Raveau, *Mater. Res. Bull.* **17,** 567 (1982).
23. J. R. Grasmeder and M. T. Weller, *J. Solid State Chem.* **85,** 88 (1990).
24. V. Caignaert, R. Retoux, C. Michel, M. Hervieu, and B. Raveau, *Physica C* **167,** 483 (1990).
25. P. Gómez-Romero, M. R. Palacín, and J. Rodríguez-Carvajal, *Chem. Mater.* **6,** 2118 (1994).